Metamaterial coatings for subwavelength-resolution imaging

Carlos J. Zapata-Rodríguez,[a] David Pastor,[a] and Juan J. Miret[b]

[a]Department of Optics, University of Valencia, Dr. Moliner 50, 46100 Burjassot, Spain;
[b]Department of Optics, Pharmacology and Anatomy, University of Alicante, P.O. Box 99, Alicante, Spain

ABSTRACT

Coating lenses are membranes made of materials exhibiting negative index of refraction and deposited on other media with high dielectric constant ε_3. Unfortunately far-field imaging suffers from centrosymmetric aberrations. We propose a simple procedure to compensate partially deviations from ray-tracing perfect imaging in asymmetric metamaterial lenses. We also show that, under some circumstances, coating superlens may recover subwavelength information transmitted in a relative spatial spectrum ranging from 1 to $\sqrt{\varepsilon_3}$.

Keywords: metamaterials, imaging, spherical aberration

1. INTRODUCTION

Asymmetric flat lenses are thin membranes made of materials exhibiting negative permittivity deposited on other media such as glass with positive dielectric constant. Using a solid substrate, this imaging device becomes mechanically stable. For silver superlenses, amplification of evanescent waves sustained by surface waves is more favorable if the real part of the dielectric constant of the metal and the substrate matches except for its sign.[1] If the lensing film shows effectively a negative permeability, negative refraction allows imaging also using homogeneous waves. Unfortunately there is no stigmatic imaging in the asymmetric arrangement and the image suffers from aberrations. In Ref. 2 it is investigated the question of inner corrections of some low-order aberrations for apertured multilayered flat lenses. However nonapertured superlenses are usually employed and oblique aberrations may be disregarded.

In the general case that the index of refraction (IR) of the output image medium is higher than that IR corresponding to the input medium surrounding the object, some evanescent waves emitted by the source become homogeneous after passing through the lens. This allows the formation of far-field images with subwavelength resolution. The transmitted spatial spectrum increases linearly upon the IR of the supporting image media, and therefore high-index materials are preferable in order to obtain an enhanced superresolution effect.

We investigate the effects of primary spherical aberration (SA) and higher-order SA in asymmetric superlenses made of metamaterials with negative IR. In Sec. 2 primary SA is corrected for a given object plane leading to residual aberrations in out-of-focus planes. Contrary to the perfect lens, this effect is in agreement with cancellation of shift invariance along the optic axis driven by asymmetry of the imaging problem. In Sec. 3 we show that the unbalanced arrangement allows proper conditions to retract backscattering. The diffractive behavior of SA-corrected metamaterial coatings are disclosed in Sec. 4. We provide the point spread function of such antireflection superlenses and we estimate the limit of resolution unambiguously. Finally we demonstrate subwavelength capabilities in far-field imaging.

2. SPHERICAL ABERRATION IN FLAT LENSES

Let us consider the asymmetric flat lens shown in Fig. 1. A point object O_1 is suspended at a distance s_1 from the front face of the superlens made of a material exhibiting negative index of refraction, $n_2 < 0$. Assuming that the object space is characterized by an index of refraction $n_1 > 0$, a real Gaussian image O_2 is formed in the metamaterial.[3] Traveling through the lens exit surface we reproduce the intermediate image at a distance s_3 provided the index of refraction n_3 of the image space turns to be positive. Note that we employ oriented axial distances, i.e. $s_1 < 0$ and $s_3 > 0$ for a real object and a real image, respectively. Also the lens width $d > 0$.

Further author information: Send correspondence to C.J.Z.R. (E-mail: carlos.zapata@uv.es)

Metamaterials VI, edited by Vladimir Kuzmiak, Peter Markos, Tomasz Szoplik, Proc. of SPIE Vol. 8070
807014 · © 2011 SPIE · CCC code: 0277-786X/11/$18 · doi: 10.1117/12.886623

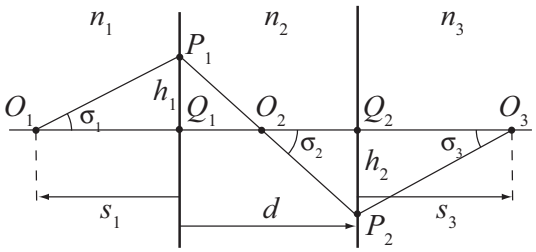

Figure 1. Schematic representation of an asymmetric flat lens of refractive index n_2 and width d.

The aberration of a ray passing through the point P_2 placed on the exit surface at a height h_2 with respect to the chief ray joining the points O_1 and O_2, and reaching the Gaussian image O_3, is estimated by the optical-path difference of both light rays, i.e. $W = n_1\left(\overline{O_1P_1} - \overline{O_1Q_1}\right) + n_2\left(\overline{P_1P_2} - \overline{Q_1Q_2}\right) + n_3\left(\overline{P_2O_3} - \overline{Q_2O_3}\right)$. This ray aberration reads approximately[4]

$$W(h_2) \approx {}_0a_{20}h_2^2 + {}_0a_{40}h_2^4 + {}_0a_{60}h_2^6\,. \tag{1}$$

The aberration terms ${}_0a_{20}$, ${}_0a_{40}$, and ${}_0a_{60}$ are attributed to defocus, primary spherical aberration (SA) and fifth-order SA, respectively. These aberration coefficients are evaluated by using the geometrical relations $\tan\sigma_1 = h_1/s_1$ and $\tan\sigma_2 = (h_1 - h_2)/d$, and the Snell law $n_1\sin\sigma_1 = n_2\sin\sigma_2$. In particular, the Gaussian image plane is given under the condition ${}_0a_{20} = 0$, which yields

$$s_3 = n_3\left(\frac{s_1}{n_1} - \frac{d}{n_2}\right)\,, \tag{2}$$

Therefore an axial displacement of the object point O_1 changing s_1 leads to an image shift following a direct proportion, as shown in Fig. 2(a). Moreover, a real image point O_3 is obtained if the intermediate image O_2 is also a real image, attained at the condition $d \geq s_1n_2/n_1$.

At the Gaussian image point O_3, where Eq. (2) is satisfied, the aberration coefficient for primary SA gives

$${}_0a_{40} = \frac{n_1n_2\left[n_1^3\left(n_2^2 - n_3^2\right)d + n_2^3\left(n_3^2 - n_1^2\right)s_1\right]}{8n_3^2(n_1d - n_2s_1)^4}\,. \tag{3}$$

Note that primary SA cannot be corrected for $0 \leq -s_1 < \infty$ whether $n_1 = n_3$ except for the perfect lens where $n_2 = -n_3$. This is a well-known case where high-order aberration coefficients also vanish leading to stigmatic imaging. Also a plane-parallel asymmetric plate may be corrected of primary SA. Provided the equation ${}_0a_{40} = 0$ is satisfied, we obtain a linear relationship between the lens width d and the object distance

$$s_1 = \frac{n_1^3\left(n_3^2 - n_2^2\right)}{n_2^3\left(n_3^2 - n_1^2\right)}d\,, \tag{4}$$

in terms of the indices of refraction of the media involved. A given flat lens cannot be corrected of primary SA for more than one object plane, as shown in Fig. 2(b). Furthermore, the primary SA coefficient diverges for the limiting case $s_3 = 0$, excepting when $n_3 \neq n_1 = -n_2$ leading to perfect imaging, corresponding to the highest absolute value of the axial parameter s_1. Therefore quality of the (real) image improves as the (real) object point O_1 come closer to the input surface.

In Figs. 2(c) and (d) we plot a ray tracing in a flat metamaterial lens of $n_2 = -2$ surrounded by object and image media of indices of refraction $n_1 = 1$ and $n_3 = 4$. Fixed the lens width d, Eqs. (2) and (4) provides the values $s_3 = 1.6d$ and $s_1 = -0.1d$, respectively. The corresponding ray tracing is shown in Fig. 2(c). Stigmatic imaging would produce a convergent focused beam of numerical aperture $n_3\sin\alpha = n_1$ leading to an angular semi-aperture $\alpha = 14.5$ deg. In our case, non-corrected high-order aberrations reduces the numerical aperture down to an effective value $\alpha_{\text{eff}} = 10.9$ deg. In order to inspect the deterioration of the image due to SA effects we also represent in Fig. 2(d) the ray tracing for a point object placed at $s_1 = -0.4d$ further from the lens entrance

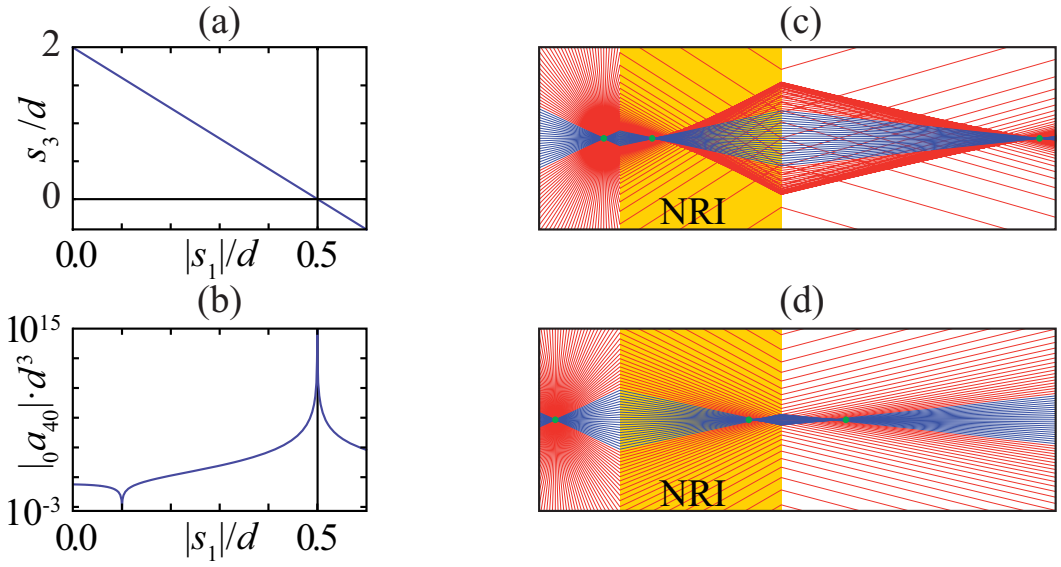

Figure 2. Geometrical imaging for a flat lens of $n_2 = -2$ sandwiched between dielectric media of indices of refraction $n_1 = 1$ and $n_3 = 4$. (a) Gaussian imaging based on Eq. (2). (b) Primary SA given by Eq. (3). On the right: Ray tracing for an object point located at (c) $s_1 = -0.1d$, which is corrected of primary SA, and (d) $s_1 = -0.4d$ from the front surface of a flat lens of width d.

surface. We observe a ray distribution that is barely confined around the Gaussian image point O_3, represented as a green dot in the image space, in opposition with the SA corrected case.

We point out that Eq. (4) provides a negative value of s_1 provided that the index of refraction n_3 in the image plane is either higher or lower than n_1 and $|n_2|$ simultaneously. In order to achieve a subwavelength effect, we pretend to transform evanescent waves emitted by the source O_1 into homogeneous wave modes in the image space. Therefore we choose a high-index dielectric $n_3 > n_1$ to register the image.

The aberration coefficient for the 5th order SA may be estimated analytically. Provided Eqs. (2) and (4) are satisfied, this high-order SA coefficient gives

$$ {}_0a_{60} = -\frac{n_1^{13}\left(n_1^2 - n_3^2\right)\left(n_2^2 - n_3^2\right)^6}{16 n_2^2 n_3^{14}\left(n_2^2 - n_1^2\right)^5 s_1^5}\,. \tag{5} $$

Therefore ${}_0a_{60}$ vanishes only for trivial solutions: (1) imaging under mirror-symmetry negative refraction on the output surface provided $n_1 \neq n_3 = -n_2$ and $s_1 = 0$, and (2) incidence of a collimated bundle of rays for which s_1 tends to infinity. Excepting these special cases, fifth-order SA cannot be corrected.

The ratio $n_3/n_1 - 1$ provides the relative enlargement of spatial bandwidth corresponding to evanescent waves in the object space which are transformed into homogeneous plane waves in the image space. This is clearly a subwavelength effect which has been exploited elsewhere.[5] In image formation this physical phenomenon leads to a superresolving effect, which will be developed in Sec. 4. On the other hand we point out that the value of n_2 is arbitrarily chosen provided it is negative. This is a degree of freedom which may be profited in order to impose any additional constraint.

3. REFLECTION AND TRANSMISSION

Let us consider the reflection and transmission of obliquely incident light onto the thin metamaterial film deposited on top of a transparent substrate in order to determine a suitable choice for the value of n_2. The reflection

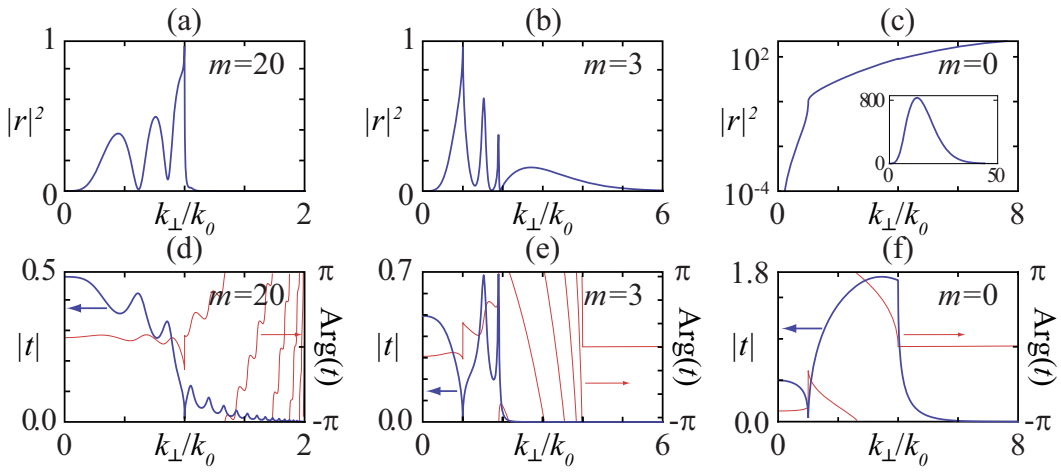

Figure 3. (a-c) Coefficient $|r|^2$ and (d-f) transmission coefficient (modulus and argument) for TE waves in a superlens of $\mu_2 = -1 + i0.001$ and $\varepsilon_2 = -4 + i0.001$. Surrounding transparent media have again indices of refraction $n_1 = 1$ and $n_3 = 4$. We consider different film widths: (a) and (d) $d = 5.125\lambda_0$, (b) and (e) $d = 0.875\lambda_0$, and (c) and (f) $d = 0.125\lambda_0$. Note that in (c) we use a logarithmic-scale axis (not in its inset).

(r) and transmission (t) coefficients evaluated from the object plane in front of the asymmetric layered lens to the image plane are[6]

$$r = \frac{r_{1,2} + r_{2,3}\exp(2i\beta_2 d)}{1 + r_{1,2}r_{2,3}\exp(2i\beta_2 d)}\exp(-2i\beta_1 s_1), \tag{6a}$$

$$t = \frac{t_{1,2}t_{2,3}}{1 + r_{1,2}r_{2,3}\exp(2i\beta_2 d)}\exp(-i\beta_1 s_1 + i\beta_2 d + i\beta_3 s_3), \tag{6b}$$

being the propagation constant

$$\beta_i = \sigma_i\sqrt{\varepsilon_i\mu_i k_0^2 - \vec{k}_\perp\cdot\vec{k}_\perp}, \tag{7}$$

where $\sigma_i = 1$ for dielectrics and $\sigma_2 = -1$ for negative-index media, $k_0 = 2\pi/\lambda_0$ is the wavenumber in vacuum, ε_i and μ_i stand for relative permittivity and permeability of the media involved, respectively, and $\vec{k}_\perp$ is the transverse wave vector, i.e. the projection of the wave vector over a plane that is parallel to each flat-lens interface. The Airy's formulae (6) depend on the reflection coefficient at a single interface,

$$r_{i,j} = \frac{\mu_j\beta_i - \mu_i\beta_j}{\mu_j\beta_i + \mu_i\beta_j}. \tag{8}$$

which is valid for s-polarized waves, and the transmission coefficient $t_{i,j} = 1 + r_{i,j}$. For the sake of brevity we will deal with p-polarized waves elsewhere.

A layer with $\beta_2 d = -(2m+1)\pi/2$ (for $m = 0, 1, 2, \ldots$) can be used to completely eliminate the reflection of light, which is intrinsically a dispersive phenomenon depending upon k_0. This is commonly denominated an antireflection coating. For that purpose we additionally impose $r_{1,2} = r_{2,3}$ in Eq. (6a) leading to $r = 0$, which is satisfied if

$$\beta_2^2\mu_1\mu_3 = \mu_2^2\beta_1\beta_3. \tag{9}$$

For normally incident light, i.e. $k_\perp = 0$, Eq. (9) is simplified as $Z_2^2 = Z_1 Z_3$, where Z_i is the intrinsic impedance of the medium i. Let us also assume that $\mu_i = \sigma_i$. Therefore we finally obtain a condition $n_2 = -\sqrt{n_1 n_3}$ involving the indices of refraction of all media. Note that the latter equation is hold in simulations shown in Fig. 2. Finally, a quarter-wave layer with $d = \lambda_2/4$ ($+m\lambda_2/2$ for $m \neq 0$), being $\lambda_2 = \lambda_0/(-n_2)$ is of our interest.

In Figs. 3(a-c) we show the reflectance $|r|^2$ evaluated for s-polarized waves and superlenses of different widths. We observe that reflection is extinguished for $k_\perp = 0$ in all cases. However reflectance may be significant for higher

spatial frequencies. Note that there is no average flow into the medium of lesser refractive index for $k_\perp > k_0$. The field intensity within this spectral domain, however, is by no means zero, and the reflection coefficient might reaches absolute values higher than unity, clearly seen in the inset of Fig. 3(c) for $m = 0$. Moreover, the time average of the flow in the object space is supported by evanescent waves that do not contribute to the far field. In Figs. 3(d-f) we also represent the transmission coefficient t in amplitude and phase. For a slab width much higher than the wavelength, the evanescent waves emitted by the source point O_1 cannot reach the entrance face and homogeneous waves satisfying $k_\perp \leq k_0$ contribute effectively to the transmitted field in the image space, as shown in Fig. 3(d) for $d = 5.125\lambda_0$. Decreasing d down to values close to λ_0 leads to the conversion of evanescent waves in medium 1 to homogeneous waves in medium 2. In Fig. 3(e) we observe a critical participation of waves with transverse spatial frequencies $k_0 < k_\perp < 2k_0$ for a lens width $d = 0.875\lambda_0$. In the limit $d = 0.125\lambda_0$ associated with $m = 0$ we increase the spatial bandwidth in the interval $2k_0 < k_\perp < 4k_0$ involving evanescent waves in media 1 and 2 which are transformed into homogeneous waves in the image space, as seen in Fig. 3(f). For that reason such a spectral stretching allows a subwavelength resolution effect in the formation of the far-field image.

4. SUPERRESOLVING IMAGE FORMATION

To determine the limit of resolution of a flat superlens we use the field distribution generated by a point object. Hakkarainen et al. calculated the PSF of the imaging system by investigating near-field imaging of a point dipole by a lossy, nanoscale metamaterial slab.[7] In this study we follow a different approach consisting of evaluating the PSF produced by a point source which is characterized by a delta function in the object plane. This is thoroughly discussed in Ref. 8 and here we only give a brief summary.

Based on the angular spectrum representation of the scattered field, for s-polarized waves, the field $\vec{E}$ in the image space may be expressed as a 2D convolution,

$$\vec{E}\left(\vec{R},z\right) = \vec{E}_{sc}\left(\vec{R}\right) * h\left(\vec{R},z\right), \tag{10}$$

where $\vec{E}_{sc}$ is the electric field excited by the source at the object plane. Strictly speaking Eq. (10) is not restricted to sources located at the object plane involving simple defocusing effects in the impulse response. Let us consider a single object point O_1 from here on. The optic z-axis containing the point O_1 and the intermediate and final image points, O_2 and O_3 respectively, is characterized by the unit vector $\hat{z}$, and therefore the transverse 2D vector $\vec{R} \perp \hat{z}$. The scalar 3D PSF

$$h\left(\vec{R},z\right) = \frac{1}{(2\pi)^2}\iint t\left(\vec{k}_\perp\right)\exp\left(i\vec{k}_\perp\vec{R}\right)\exp\left(i\beta_3 z\right)d\vec{k}_\perp, \tag{11}$$

is derived by means of the transmission coefficient between the object plane and the conjugate image plane given in Eq. (6b). Note that $h(\vec{R}, z > 0)$ for $t = 1$ represents the propagator of the first Rayleigh-Sommerfeld integral and it is related with a divergent wave which focus is placed in the center of the image plane $z = 0$.[9]

For symmetric flat lenses where $n_1 = n_3$, Eq. (10) may be set as a 3D convolution in virtue of its property of shift invariance along the z-axis. However asymmetric flat lenses are not invariant under displacements on the optic axis. This is in agreement with our discussion in Sec. 2 concerning SA correction, which is achieved in a unique object plane. In fact, the transmission coefficient t given in Eq. (6b) varies when the distance s_1 from the flat lens to the object plane changes and so the 3D PSF h does accordingly.

The integrand in Eq. (11) is radially symmetric so that the evaluation of the 3D PSF is simplified as[8]

$$h\left(R,z\right) = \frac{1}{2\pi}\int_0^\infty t\left(k_\perp\right)J_0\left(k_\perp R\right)\exp\left(i\beta_3 z\right)k_\perp dk_\perp, \tag{12}$$

where the radial coordinate $R = |\vec{R}|$, and J_0 is the Bessel function of the first kind and of order 0. In Fig. 4 we represent the 3D PSF for a negative-index lens of $\mu_2 = -1 + i0.001$ and $\varepsilon_2 = -4 + i0.001$ and different widths, which is sandwiched in media of IR $n_1 = 1$ and $n_3 = 4$. The object point O_1 is placed at a distance $s_1 = -0.1d$ given by Eq. (4) to correct primary SA. We compute the impulse response within the interval

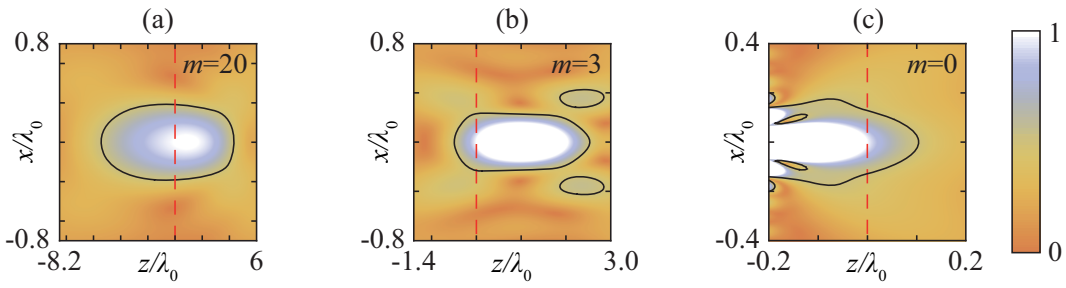

Figure 4. Magnitude of the PSF $|h|$ within $z \geq -s_3$ for a negative-index slab with $\mu_2 = -1 + i0.001$ and $\varepsilon_2 = -4 + i0.001$ and different widths $d = \lambda_2/4 + m\lambda_2/2$: (a) $d = 5.125\lambda_0$, (b) $d = 0.875\lambda_0$, and (c) $d = 0.125\lambda_0$. The density plots are normalized to unity at the paraxial image point $(x, z) = (0, 0)$. The solid line indicates points where amplitude falls off 1/2. The dashed red line marks the Gaussian image plane.

$z \geq -s_3$ constituting the real image space. The amplitude distribution of the PSF for a slab width d below the wavelength shows a behavior different than the impulse response for $d \gg \lambda_0$. For instance, if $d = 5.125\lambda_0$ shown in Fig. 4(a), the FWHM of the PSF in the geometrical image plane yields $\Delta_x = 0.778$ in units of λ_0, which is close to the wavelength. Moreover, the amplitude maximum is found far from the output interface quite close to the image plane. Nevertheless a small axial shift of 0.989 λ_0 is encountered in opposite direction to the lens driven by residual high-order aberrations. Additionally the FWHM along the z-axis may be evaluated in this case giving $\Delta_z = 9.77$, also in units of λ_0. Fig. 4(b) illustrates the diffraction behavior of a thinner film in the case $d = 0.875\lambda_0$. The limit of resolution has decreased substantially both in the transverse direction, $\Delta_x = 0.476$, and along the optic axis, $\Delta_z = 3.03$. According to Fig. 3(e), this superresolving response may be attributed to evanescent waves in medium 1 that are converted into homogeneous waves in medium 2, which belong to the spectral range $k_0 < k_\perp < 2k_0$, and contributes effectively to the wave field in the image. However, wave aberrations introduce a spatial blurring of the PSF restraining an improved resolution. This argument also sustains the significant on-axis shift of 1.036 λ_0 of the spot maximum getting far from the superlens. Finally, when $d = 0.125\lambda_0$ then $\Delta_x = 0.273$, denoting a limit of resolution well below λ_0. Note that in the imaging process, the record of the subwavelength details are associated with spatial frequencies higher than k_0. Moreover, those frequencies surpassing $4k_0$ fall off fast in the transit from the output plane of the lens toward the image plane, thus frustrating a 3D focusing.[10]

5. CONCLUSIONS

We conclude that the effects of SA may be alleviated in asymmetric superlenses made of negative-index metamaterials. Primary SA is straightforwardly corrected for a given object plane. However residual aberrations come out in other Gaussian conjugate planes. This effect is in agreement with cancellation of shift invariance along the optic axis driven by asymmetry of the imaging problem. Moreover, the diffractive behavior of SA-corrected metamaterial claddings is clearly improved by considering proper conditions to retract backscattering. By means of the PSF of such antireflection imaging coatings we are able to estimate the limit of resolution unambiguously. Finally we demonstrate far-field imaging may recover sub-λ information concerning evanescent waves launched by the object. Proximity of the source from the entrance surface of the lens, and the latter from the exit interface in comparison with the wavelength are crucial in order to exhibit a subwavelength resolution.

ACKNOWLEDGMENTS

This research was funded by Ministerio de Ciencia e Innovación (MICIIN) under the project TEC2009-11635.

REFERENCES

1. S. A. Ramakrishna, J. B. Pendry, D. Schurig, D. R. Smith, and S. Schultz, "The asymmetric lossy near-perfect lens," *J. Mod. Opt.* **49**, pp. 1747–1762, 2002.

2. Z. Lin and Y. Zou, "Low-order aberration corrections of multilayer flat lenses using negative-index materials," *Appl. Opt.* **45**, pp. 6925–6931, 2006.
3. V. G. Veselago, "The electrodinamics of substances with simultaneously negative values of ϵ and μ," *Physics-Uspekhi* **10**(4), p. 509, 1968.
4. V. N. Mahajan, *Optical imaging and aberrations. Part I. Ray geometrical optics*, SPIE Press, Bellingham, 1998.
5. N. Calander, "Surface plasmon-coupled emission and Fabry-Perot resonance in the sample layer: A theoretical approach," *J. Phys. Chem. B* **109**, pp. 13957–13963, 2005.
6. P. Yeh, *Optical Waves in Layered Media*, Wiley, New York, 1988.
7. T. Hakkarainen, T. Setälä, and A. T. Friberg, "Subwavelength electromagnetic near-field imaging of point dipole with metamaterial nanoslab," *J. Opt. Soc. Am. A* **26**, pp. 2226–2234, 2009.
8. C. J. Zapata-Rodríguez, D. Pastor, and J. J. Miret, "Three-dimensional point spread function and generalized amplitude transfer function of near-field flat lenses," *Appl. Opt.* **49**, pp. 5870–5877, 2010.
9. M. Nieto-Vesperinas, "Problem of image superresolution with a negative-refractive-index slab," *J. Opt. Soc. Am. A* **21**, pp. 491–498, 2004.
10. R. Marques, M. J. Freire, and J. D. Baena, "Theory of three-dimensional subdiffraction imaging," *Appl. Phys. Lett.* **89**, p. 211113, 2006.